The concept of X-ray CT dose evaluation method using radiochromic film and film-folding phantom

Nobuyoshi Tanki[1,2], Toshizo Katsuda[3], Rumi Gotanda[4], Tatsuhiro Gotanda[4], Shinya Imai[5], Yasuyuki Kawaji[6], Atsushi Noguchi[7], Tadao Kuwano[8], Hideki Fujita[9], Yoshihiro Takeda[1]

[1]Department of Radiological Technology, Graduate School of Health Sciences, Okayama University, 2-5-1 Shikata-cho, Kita-ku, Okayama 700-8558, Japan

[2] Brain Activity Imaging Center, ATR-Promotions Inc., 2-2-2 Hikaridai, Sorakugun Seika-cho, Kyoto 619-0288, Japan.

[3] Department of Medical Radiation Sciences, Shizuoka College of Medicalcare Science, 2000 Hiraguchi, Hamakita-ku, Hamamatsu, 434-0041 Shizuoka, Japan

[4] Department of Radiological Technology, Faculty of Health Science and Technology, Kawasaki University of Medical Welfare, 288 Matsushima, Kurashiki, 701-0193 Okayama, Japan

[5] Department of Radiological Science, Faculty of Health Science, Morinomiya University of Medical Sciences, 1-26-16 Nankou-kita, Suminoe-ku, 559-8611 Osaka, Japan

[6] Department of Radiological Science, Faculty of Health Sciences, Junshin Gakuen University, 1-1-1 Chikushioka, Minami-ku, 815-8510 Fukuoka, Japan

[7] Aoi Hospital, Medical Incorporated Association Seishokai, 6-14-2 Aramaki, Itami, 664-0001 Hyogo, Japan

[8] Osaka Center for Cancer and Cardiovasucular Disease Prevention, 1-6-107 Morinomiya, Joutou-ku, 536-8588 Osaka, Japan

[9] Department of Radiation Oncology, Osaka Saiseikai Nakatsu Hospital, 2-10-39 Shibata, Kita-ku 530-0012 Osaka, Japan

Author to whom correspondence should be addressed:

Nobuyoshi Tanki

Brain Activity Imaging Center, ATR-Promotions Inc.

2-2-2 Hikaridai, Sorakugun Seikacho, Kyoto 619-0288, Japan.

E-mail: n-tanki@baic.jp

Running title: X-ray CT dosimetry with RCF

Acknowledgments

This work was supported by JSPS KAKENHI Grant Number 17K10380. We would like to thank Editage for English language editing.

Abstract:

In this paper, we propose a novel RCF-based CT dosimetry method, which is different from the method based on CT dose index. RCF dosimetry using Gafchromic QA2 films was performed using two lengths of film-folding phantoms. The phantom was exposed to X-ray CT through a single scan, while the RCF was sandwiched between the phantoms. We analyzed the dose profile curve in two directions to investigate the dose distribution. We observed a difference in the dose distribution as the phantom size changed. Our results contradict with the results of previous studies such as Monte Carlo simulation or direct measurement. The ability to visually evaluate 2D dose distributions is an advantage of RCF dosimetry over other methods. This research investigated the ability of 2D X-ray CT dose evaluation using radiochromic film and film-folding phantom.

Key words

Computed tomography, film-folding phantom, XR-QA2, radiochromic film, 3D dosimetry

Introduction

In recent years, one of the main concerns regarding X-ray computed tomography (CT) examinations is reducing radiation exposure while maintaining diagnostic quality. De González and Darby [1] argued that 3.2 % of all cancer cases in Japan were induced by exposure to diagnostic X-ray examinations. As radiation exposure during CT is higher than that during chest or head radiography [2], accurate dose evaluation of X-ray CT examinations becomes extremely important for ensuring patient safety.

In general, the CT dose index (CTDI) and related measurement indexes were used for X-ray CT dose evaluation. Although CTDI is useful for predicting X-ray exposure during CT examination, it cannot retrieve the dose delivered to patients. In addition, CTDI is calculated based on measurements obtained from phantoms with diameters of 16 and 32 cm for adult heads and bodies, respectively. [3] CTDI is calculated from the measurement values using an ion chamber. Ion chambers are widely used for dose measurement in X-ray CT. However, they integrate doses over a certain length, and their spatial resolution is very low. In addition, the CTDI does not allow measurement at any location such as on the surface of the object.

As an alternative to CTDI evaluation, thermoluminescent dosemeters (TLDs) were used for CT dosimetry. [4], [5] Due to their small size, TLDs can be placed at various location such as on the surface or inside the subject. The appropriately calibrated TLDs provide reliable dose measurements. However, the dosimetry using TLDs is time-consuming work. These dosimetry techniques cannot obtain contiguous dose distributions owing to their inherent characteristics.

In recent years, polymer gel dosimetry has focused as one of 3D dosimetry method. Lots of researchers focus on dose evaluation of radiation therapy, a few researchers try to measure radiation dose of X-ray CT [6] [7] The current limitation of this dosimetry is the minimum detectable dose [8]. If this problem is solved, it might be a useful tool for CT dosimetry.

A radiochromic film (RCF) obtains two-dimensional (2D) dose information with high spatial resolution. These 2D measurements obtain precise dose distributions with direct and scatter radiation. This feature is not found in other dosimetry methods. Devic et al. [9] have published a detailed technical overview of RCF dosimetry. Tomic et al. investigated RCF application in X-ray CT dosimetry. They mainly studied the methodologies and protocols of dosimetry methods using RCFs. [10] [11] [12] These studies focused on using RCFs for performing dosimetry in the diagnostic X-ray energy range.

Gotanda developed a novel phantom for 3D dosimetry using RCF. [13] [14] This phantom consists of a vinyl chloride sheet rolled into a cylinder; the phantom diameter, dose measurement position, and users can determine the depth arbitrarily. With these features, this phantom can be used for both dose measurements in X-ray CT and complex radiation therapy techniques. However, this method needs several RCFs to develop image scanning methods and image analysis applications for examining complicated data. We have developed film-folding phantoms for use in 3D X-ray CT dosimetry. [15] The film-folding phantom facilitates relatively easy acquisition of 3D X-ray CT dose distributions. This novel method may be able to perform precise measurements including the separation of direct and scatter radiation that could not be achieved with CTDI.

The purpose of this study was to investigate a novel X-ray CT dosimetry method using an RCF and a film-folding phantom. We also mention the application of this method for 3D dosimetry.

Materials and Methods

Design of film-folding phantom and concept of 3D dosimetry

All components of the film-folding phantoms comprising two semicylinders were made from polymethyl methacrylate. Five phantoms with different diameters (8, 10, 12, 14, and 16 cm) were procured from WBI Co., Ltd. (Neyagawa, Japan). The long-axis length of all phantoms was 30 cm.

The representative phantom form with the two parts attached is shown in figure 1. During radiation exposure, the RCF was sandwiched and tightly fixed between the semicylinders. The phantom was held on a CT bed to which the two semicylinders were attached, and the centerline was located along the isocenter of the CT gantry.

The cylindrical phantom was designed to measure 360° radiation exposure. Its shape is similar to that of a CTDI measurement phantom. However only a small area can be measured using an ion chamber or glass luminescent dosemeter, and it takes a long time to measure the entire exposure range. This problem will be solved using an RCF, which can obtain 2D dose distributions. In a single scan, unless the exposure conditions are changed for each exposure direction, the dose distribution in a certain cross section should be the same in any direction on the ideal situation without attenuation materials. Then, combining dose distributions in multiple directions gives a virtual 3D dose distribution. Therefore, the 2D dose analysis results were the same the 3D dose analysis results.

To measure actual 2D dose distributions using the film-folding phantom, the RCF was placed on the plane of the lower semicylinder and sandwiched by the other semicylinder. The centre of the transverse plane was aligned with the rotational centre of the X-ray source using the positioning laser of the X-ray CT system. Then, the sandwiched RCF was exposed during CT examination.

This technique was able to obtain radiation dose measurements in various scan techniques such as single, helical, or cone-beam X-ray CT scan, and provided a virtual 3D dose distribution.

Exposure procedure and RCF scanning

Dosimetry performed using our proposed phantom was not verified. Therefore, we performed experiments to confirm the dose distribution changes caused by the different phantom diameters. In this study, we compared two different phantoms with diameters of 10 (infant’s head) and 16 cm (adult head).

The exposed RCF was a Gafchromic XR-QA2 film (lot number: 01041702, exposure date: January 2019, Ashland, Inc., Covington, LA, USA). The RCF was cut out 5 mm larger than the size of phantom, and discarded data outer region than the edge of phantom.

The RCF was exposed using a clinical X-ray CT system (Aquilion Lightning; Canon Medical Systems, Ohtawara, Japan). The starting point of X-ray exposure could not be fixed owing to mechanical limitations. The experimental setup is illustrated in figure. 2.

The exposure parameters for X-ray CT were set as follows: tube voltage of 120 kVp, tube current of 300 mA, slice thickness of 20 mm, time per gantry rotation of 1 s for 10-cm and 2 s for 16-cm phantoms. To simplify the interpretation of the acquired data, we only used stepwise scanning.

We used a commercial image scanner (Epson ES-10000G, Seiko Epson Co., Nagano, Japan) to digitize the RCFs. In the digitizing process, Moiré artefact commonly arise from partial reflections at the RCF–glass bed interface of the scanner [16] [17]. This artefact interferes with the data analysis. To remove the Moiré artefact, a protective film with liquid crystal display (LCD-230W; Sanwa Supply Inc., Okayama, Japan) was placed over the reading face of the scanner. [18] [19] The films were read with a 48-bit, 150-dpi resolution (0.169 mm/pixel) in RGB mode. From the scanned images, we separated red, green, and blue channels and used the red channel data by owing to the high sensitivity of this channel for lower radiation doses. [20] [21] To eliminate the noise due to the yellow polyester layer, the subtraction images were calculated using the scanned images before and after exposure. [22]

Dose-calibration curves

The absorbed doses were measured by the semiconductor dosemeter (NOMEX multimeter; PTW Inc., Freiburg, Germany) to verify the relationship between the exposure dose and pixel value changes in the RCF. The dose-calibration curves were calculated using Kaleida Graph 4.0 (HULINKS Inc.; Tokyo, Japan). The data were collected from 25 mGy to 200 mGy at 80, 100 and 120 kVp to confirm energy dependence, and the dose-calibration curve at 120 kV was created to calculate the dose distribution. The dose-calibration curve was fitted using the following equation:

$$y = a + b \cdot e^{cx} \quad (1)$$

Selection of the fitting function referred to previous studies. [10] [23] [24]

Profile curve analysis for two axis directions

Image processing and analysis were carried out using ImageJ version 1.52 (National Institutes of Health, Bethesda, MD, USA). We performed the pseudo colour map and profile curves to analyze the pixel intensity distribution of the RCF. [25] [26] Figure 3(a) shows the scanned image of the exposed RCF for the 10-cm-diameter phantom obtained using ImageJ on the rainbow smooth lookup table (LUT). In this LUT, cold colour areas indicate strong X-ray exposure, and warm colour areas indicate weak X-ray exposure. In short, the blue area indicates the RCF area exposed to direct X-rays, whereas the green and yellow areas indicate the RCF area exposed to scattered X-rays.

Along the long axis, the profile curves were drawn from three lines shown in figure 3(b). The profiles were set at the centre and both ends at 3.71 cm from the centre. Line B was determined as the centre of the scanned image in the short-axis direction. We hypothesized that the dose differences appeared between the centre and both ends. Along the short axis, the profile curves were drawn using seven lines shown in figure 3(c). In this direction, the profile curves were set at the centre and both ends of the direct exposure region; they also included the proximal and distal areas from the direct exposure region that were exposed to scattered radiation. Line G was determined as the centre with a width equal to 25% of the exposed area, calculated from the minimum pixel value on profile curve B. In the case of the 16-cm-diameter phantom, the profile curves were measured at values equal to 1.5 times the positions used for the 10-cm-diameter phantom.

Results

Dose-calibration curves

To evaluate quantitatively the results in this study, pixel values of the RCF scanned images were converted to absorbed doses. Figure 4 shows the relationship between the dose measurements obtained using the semiconductor dosemeter and pixel values of the subtraction images. The equation of the dose-calibration curve is already described in paragraph 2.C. The parameters set for equation (1) were as follows: $a = 15; b = 5.4677 \times 10^{-2}; c = 1.9542 \times 10^{-4}$. The coefficient of determination (r^2) was 0.99477. The solid line represents the dose-calibration curve at 120 kVp. The energy dependence of the tube voltage shows the same tendency as that observed in previous studies. [25] [26] The dose-calibration curve at 100 kVp was fitted with the same parameters ($r^2 = 0.98817$) at 120 kVp, but the parameters were changed for 80 kVp ($a = 15; b = 1.1540 \times 10^{-2}; c = 2.2973 \times 10^{-4}; r^2 = 0.9961$).

Profile curve analysis for two axis directions

To confirm the dose distribution in a certain plane, the profile curves were measured along two directions. The measurement positions are described in paragraph 2.D.

First, figure 5 shows the dose distribution maps obtained using the phantoms having diameters of 10 and 16 cm. To compare these dose distributions, the maximum and minimum values were set 50 and 0 mGy, respectively. These results reflect the differences in the dose distributions caused by the phantom sizes. The maximum and minimum values of the lookup table were unified to compare the dose distributions in two phantoms with different diameters, in figure 5. In reality, the dose in white region in figure 5(b), i.e., the area exposed to direct radiation, reached up to 180 mGy.

Second, the profile curves for each phantom and directions were drawn. The profile curves along the long axis are shown in figure 6. It can be seen that the 16-cm-diameter phantom shows a higher dose at the skirts of the profile curve and a larger dose difference between the centre and edge of the slice. Moreover, the maximum value of the ratio between the centre and periphery increases as the size of the phantom increases. For example, A/B and C/B with the 10-cm-diameter phantom were 1.15 and 1.26, respectively, while A/B and C/B with the 16-cm-diameter phantom were 1.68 and 1.67, respectively.

Figure 7 shows the profile curves along the short axis. The data presented are mainly from two parts, i.e. the direct (positions F, G, and H) and scattered radiation exposure areas (positions D, E, I, and J). For both the phantom

sizes, the doses at the peripheral regions in the phantoms were higher than those in the central region. These results seem like a contradiction in terms with the results of previous studies such as Monte Carlo simulation or direct measurement. [27] However, another research reported the centre dose was increased and the surface doses were decreased with decreasing phantom size [28] [29]. It should be noted that the relationship between the central and peripheral doses varies with the size of the phantom. The doses at positions D and J did not depend on the size of the phantom; however, the doses at positions E and I differed by approximately three times. In figure 7(b), the profile curves show that the maximum dose positions are deeper than the phantom surface. Local dose changes observed in both the profile curves are due to RCF-related factors such as scratches or artefacts.

Discussion

The goal of this study was to assess the possibility of 3D X-ray CT dosimetry using RCFs. To accomplish this purpose, we performed two experiments using a Gafchromic XR-QA2 film and two different-sized phantoms. Discussed below are two aspects regarding the practical applications of X-ray CT dose evaluation using RCFs.

Uncertainty of dose calibration at low energy

As explained in paragraph 3.A, the calibration curves changed with tube voltage when using Gafchromic XR-QA2. Other researchers who performed CT slice profile measurements using RCFs have also used XR-QA or XR-QA2 [30] [31] [32]. The estimated doses in this research is reasonable compared to those estimated in previous research [33]. However, RCF dosimetry in X-ray CT has dose estimation uncertainties at low X-ray energies. The sensitivity of RCFs to X-ray energy depends on the types of RCFs used. For example, RCFs such as Gafchromic XR-QA2, Gafchromic EBT3, and XR-RV3 are suitable for measurements in the kilovolt range. Hwang and colleagues investigated the dosimetry of X-ray mammography using XR-QA2, and they reported dose overestimation within the acceptable range in clinical application. [34] Moreover, Massillon et al. mentioned that uncertainties are affected by the film model, phantom material, and probably by ionization density based on experiments conducted using Gafchromic EBT3 and MD-V3. [35] Ruiz-Morales et al. reported that dosimetry protocols or recalibration processes affect the accuracy of RCF dosimetry. [36] Thus, these findings indicate that improving the calibration accuracy is necessary to perform actual RCF dosimetry measurements at low X-ray energies. Overcoming this problem is the objective of our future research. Furthermore, our results will be necessary to verify the effectiveness of our method with other types of RCFs to estimate doses accurately.

Comparison to previous study and towards 3D dosimetry

We used the profile curves in two directions to investigate dose distributions. Although the profile curves only provide information based on a specific line, the dose distribution map enables detailed quantitative and qualitative evaluation.

In figure 5, the dose distributions of the two phantoms are different. First, to compare the previous report using phantom for CTDI measurement [29], the tendency for the diameter of the phantom to affect the ratio of central to peripheral doses is consistent with the results shown in Fig. 7. In another previous research, [23] dose profile curves of

X-ray CT were measured using silicon photodiodes with two phantoms having lengths of 140 and 900 mm. These results suggested that the phantom length and measurement area should be appropriately large for measuring dose equilibrium. The 2D visualization of radiation effects is an additional advantage of using RCF dosimetry. The difference between the two distributions was attributed to the effect of the phantom size; our method could easily measure the dose quantitatively according to the subject size by changing the size of the phantom. In another study, [37] Tsai et al. measured dose profiles of a single CT scan; they could separate the results of the primary beam and scattered radiation. Applying their method, X-ray CT dosimetry using an RCF can separate the contribution of the two radiations.

As shown in figure 6, the doses at the direct exposure area on the inner and front parts against the CT gantry were different. These dose differences are evident in figure 6(a). Along the short axis, radiation scattering caused by the phantom altered the dose distributions. The imbalance between the left and right portions of the direct exposure area in figure 7 (profile curves F and H) can be observed in figure 6. We inferred that radiation scattering depended on the phantom and its size [38] or shape. Though we obtained some profile curves to confirm the dose distribution, the ability to visually evaluate 2D dose distributions is an advantage of RCF dosimetry over other methods. Because the data in 2D dose distributions are the same in any direction passing through the centre of the phantom, they include a part of the data present in 3D dose distributions. Based on this principle, 3D dose distributions can be reconstructed from 2D planar dose information. RCF dosimetry retrieves 3D dose distributions and detailed dose evaluation can be performed, which is not possible when using CTDI. However, in actuality, it is necessary to take into account the X-ray attenuation caused by the bed or other factors. Development of reconstruction algorithms, verification of 3D dose distributions, and application of RCF dosimetry in helical or cone-beam scanning are major challenges associated with quantitative dose evaluation. Moreover, in this study, we did not verify the calculation algorithm of 3D dose distributions.

One of the limitations of our study is with regard to evaluating the validity of the dose estimates. The tendency of profile curves shown in figure 6 and 7 contradict with the results of previous studies using Monte Carlo simulation or other dosemeters. However, this phenomenon is not due to a measurement failure. The same tendency was observed in all experiments using the RCF in our study. We believe that this is due to the beam hardening effect. However, there are no highly absorbent substances in the phantom except for RCF. It is unlikely that the size and

material of the phantom will have a strong beam hardening effect. This may be due to the influence of the direction-dependent on the RCF as well; however, additional experiments are needed to confirm this hypothesis.

Conclusion

In this research, we proposed the concept of RCF dosimetry for evaluation of 3D X-ray CT dose distributions. The uncertainty in converting pixel values to doses is a problem when using RCF dosimetry in X-ray CT performed using kilovolt radiation. We studied the concept of 3D X-ray CT dosimetry and the advantages of 2D dose evaluation. Our multidimensional RCF dosimetry procedure will provide detailed radiation exposure information.

Conflicts of interest

The authors declare no conflicts of interest regarding the publication of this paper.

References

1. de González AB, Darby S. Risk of cancer from diagnostic X-rays: estimates for the UK and 14 other countries. *Lancet*. **363**(9406), 345–351 (2004)

2. United Nations Scientific Committee on the Effects of Atomic Radiation (UNSCEAR). Sources and effects of ionizing radiation. New York: United Nations (2000)

3. Bauhs JA, Vrieze TJ, Primak AN, Bruesewitz MR, McCollough CH. CT dosimetry: comparison of measurement techniques and devices. *Radiographics*. **28**(1), 245–253 (2008)

4. Hall JL, Navarrete JL, Surprenant E, Sklansky J, Eisenman JI. A new TLD-phantom measurement system for determining dose distribution levels in the right and left breast from spiral CT chest imaging. *J Appl Clin Med Phys*. **3**(4), 324–327 (2002)

5. Mege JP, Wenzhao S, Veres A, Auzac G, Diallo I, Lefkopoulos D. Evaluation of MVCT imaging dose levels during helical IGRT: comparison between ion chamber, TLD, and EBT3 films. *J Appl Clin Med Phys*. **17**(1), 143–157 (2016)

6. Hilts M, Audet C, Duzenli C et al. Polymer gel dosimetry using x-ray computed tomography: a feasibility study. *Phys Med Biol. 45*(9), 2559-2571. (2000).

7. Trapp JV, Bäck SÅJ, Lepage M et al. An experimental study of the dose response of polymer gel dosimeters imaged with x-ray computed tomography. *Phys Med Biol.* 46(11), 2939-2951. (2001).

8. Shih TY, Hsieh BT, Yen TH et al. Sensitivity enhancement of methacrylic acid gel dosimeters by incorporating iodine for computed tomography scans. *Phys Med.* 63, 1-6. (2019)

9. Devic S, Tomic N, Lewis D. Reference radiochromic film dosimetry: review of technical aspects. *Phys Med*. **32**(4), 541–556 (2016)

10. Tomic N, Quintero C, Whiting, BR et al. Characterization of calibration curves and energy dependence GafChromic™ XR-QA2 model based radiochromic film dosimetry system. *Med Phys*. **41**(6), 06210 (2014)

11. Tomic N, Devic S, DeBlois F, Seuntjens J. Reference radiochromic film dosimetry in kilovoltage photon beams during CBCT image acquisition. *Med Phys*. **37**(3), 1083–1092 (2010)

12. Boivin J, Tomic N, Fadlallah B, DeBlois F, Devic S. Reference dosimetry during diagnostic CT examination using XR−QA radiochromic film model. *Med Phys*. **38**(9), 5119–5129 (2011)

13. Gotanda, R, Katsuda, T, Gotanda, T et al. Computed tomography phantom for radiochromic film dosimetry. *Australas Phys Eng Sci Med*. **30**(3), 194–199 (2007)

14. Gotanda R, Katsuda T, Gotanda T, et al. Dose distribution in pediatric CT head examination using a new phantom with radiochromic film. *Australas Phys Eng Sci Med*. **31**, 339–344 (2008)

15. Katsuda T, Gotanda R. Dose measuring method and phantom, and X-ray image picking-up device used for the dose measuring method. WIPO patent application WO/2008/087952.

16. Gluckman GR, Reinstein LE Comparison of three high-resolution digitizers for radiochromic film dosimetry. *Med Phys*. 29(8), 1839-1846. (2002)

17. De Puysseleyr A, Srivastava RP, Paelinck L et al. Evaluation of a glassless photographic film scanner for high-gradient radiochromic film dosimetry. *Phys Med Biol.* 57(1), 127-142. (2011)

18. Gotanda T, Katsuda T, Gotanda R, et al. Evaluation of effective energy using radiochromic film and a step-shaped aluminum filter. *Australas Phys Eng Sci Med*. **34**(2), 213–222 (2011)

19. Katsuda T, Gotanda R, Gotanda T, et al. Ultraviolet ray irradiation duration for the pre-exposure of Gafchromic EBT2. *Pol J Med Phys Eng*. **24**(4), 189–193 (2018)

20. Lewis D, Micke A, Yu X, Chan MF. An efficient protocol for radiochromic film dosimetry combining calibration and measurement in a single scan. *Med Phys*. 39(10), 6339–6350 (2012)

21. Chang L, Ho SY, Lee TF, et al. Calibration of EBT2 film using a red-channel PDD method in combination with a modified three-channel technique. *Med Phys*. **42**(10), 5838–5847 (2015)

22. Gotanda R, Katsuda T, Gotanda T, et al. Temporal characterization of the flat-bed scanner influencing dosimetry using radiochromic film. *IFMBE Proc*. 68, 537–539 (2019)

23. Giaddui T, Cui Y, Galvin J, et al. Characteristics of Gafchromic XRQA2 films for kV image dose measurement. *Med Phys*. 39(2), 842–850 (2012)

24. Lillo FD, Mettlvler G, Sarno A et al. Energy dependent calibration of XR-QA2 radiochromic film with monochromatic and polychromatic x-ray beams. *Med Phys*. 43(1), 583–588 (2016)

25. Mori S, Endo M, Nishizawa K, et al. Enlarged longitudinal dose profiles in cone-beam CT and the need for modified dosimetry. *Med Phys*. 32(4), 1061–1069 (2005)

26. Anam C, Haryanto F, Widita R, et al. Scatter index measurement using a CT dose profiler. *J Med Phys Biophys*. 4, 95–102 (2017)

27. Haba T, Koyama S, Ida Y. Influence of difference in cross-sectional dose profile in a CTDI phantom on X-ray CT dose estimation: a Monte Carlo study. *Rad. Phys. Technol*. 7(1), 133–140 (2014)

28. Gotanda R, Katsuda T, Gotanda T et al. Dose distribution in pediatric CT abdominal examination: phantom study. In World Congress on Medical Physics and Biomedical Engineering, September 7-12, 2009, Munich, Germany (pp. 45-48). Springer, Berlin, Heidelberg. (2009).

29. Nickoloff EL, Dutta AK, Lu ZF. Influence of phantom diameter, kVp and scan mode upon computed tomography dose index. *Med Phys.* 30(3), 395-402. (2003)

30. Martin CJ, Gentle DJ, Sookpeng S et al. Application of Gafchromic film in the study of dosimetry methods in CT phantoms. J. *Radiol. Prot*. 31(4), 389–409 (2011)

31. Jackson SR, Ahmad S, Hu Y, Ruan C. Evaluation of different techniques for CT radiation profile width measurement. *J App Clin Med Phys*. 14(4), 4122 (2013)

32. Li B, Behrman H. An investigation into factors affecting the precision of CT radiation dose profile width measurements using radiochromic films. *Med Phys*. 42(4), 1763–1772 (2015)

33. Pearce MS, Salotti JA, Little MP et al. Radiation exposure from CT scans in childhood and subsequent risk of leukaemia and brain tumours: a retrospective cohort study. *Lancet* 380(9840), 499–505 (2012)

34. Hwang YS, Lin YY, Cheung YC, Tsai HY. Three-dimensional dose distribution in contrast-enhanced digital mammography using Gafchromic XR-QA2 films: Feasibility study. *Rad Phys Chem*. 104, 204–207 (2014)

35. Massillon-Jl G, Cabrera-Santiago A, Xicohténcatl-Hernández N. Relative efficiency of Gafchromic EBT3 and MD-V3 films exposed to low-energy photons and its influence on the energy dependence. *Phys Med*. 61, 8–17 (2019)

36. Ruiz-Morales C, Antonio Vera-Sánchez J, González-López A. Optimizing the recalibration process in radiochromic film dosimetry. *Phys Med Biol*. 65(1), 015016 (2020)

37. Tsai HY, Tung CJ, Huang MH, Wan YL. Analyses and applications of single scan dose profiles in computed tomography. *Med Phys*. 30(8), 1982–1989 (2003)

38. Anam C, Haryanto F, Widita R, et al. Scatter index measurement using a CT dose profiler. *J Med Phys Biophys*. 4, 95–102 (2017)

Figures

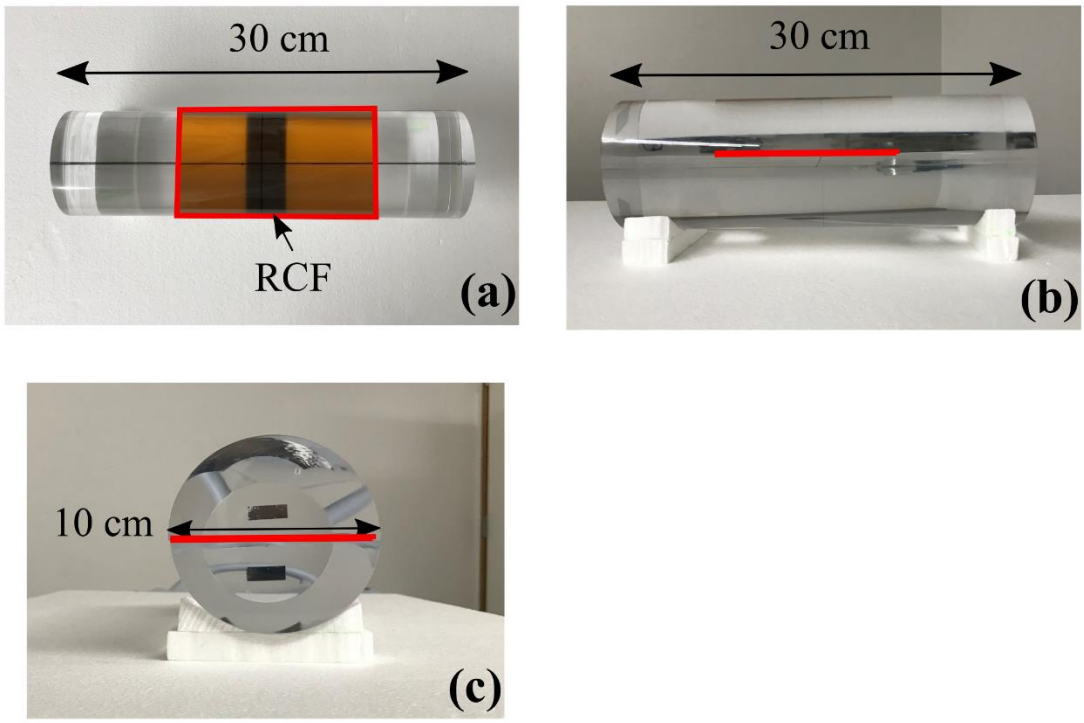

Fig. 1. Views of fabricated film-folding phantom with 10-cm diameter from the top (a), side (b), and front (c). The red line indicates the RCF location in the phantom.

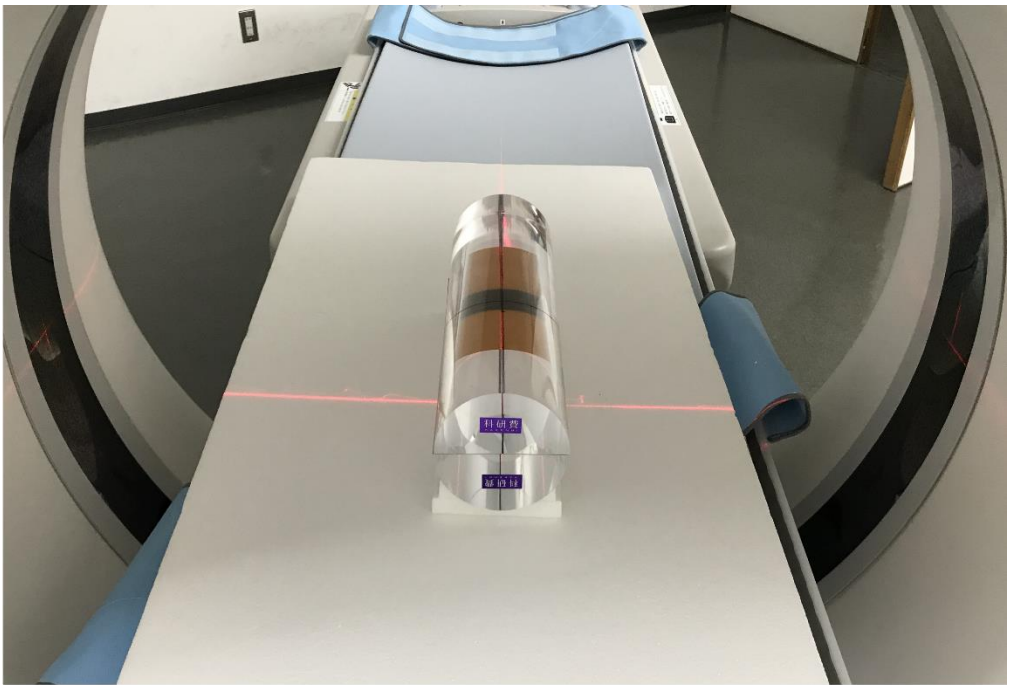

(a)

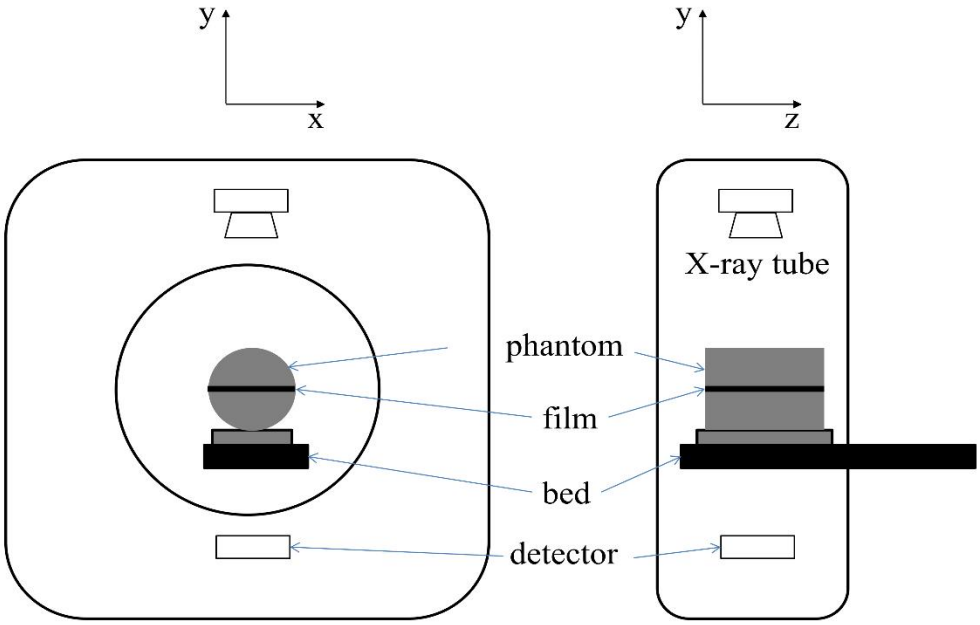

(b)

Fig. 2. Photograph of experimental setup (a) and its diagram (b). The axial slice plane is defined as the *x*–*y* plane, and the direction of slice thickness is defined as the *z* axis. We define the plane parallel to the *x*–*y* plane as the short axis and the plane parallel to the *y*–z plane as the long axis.

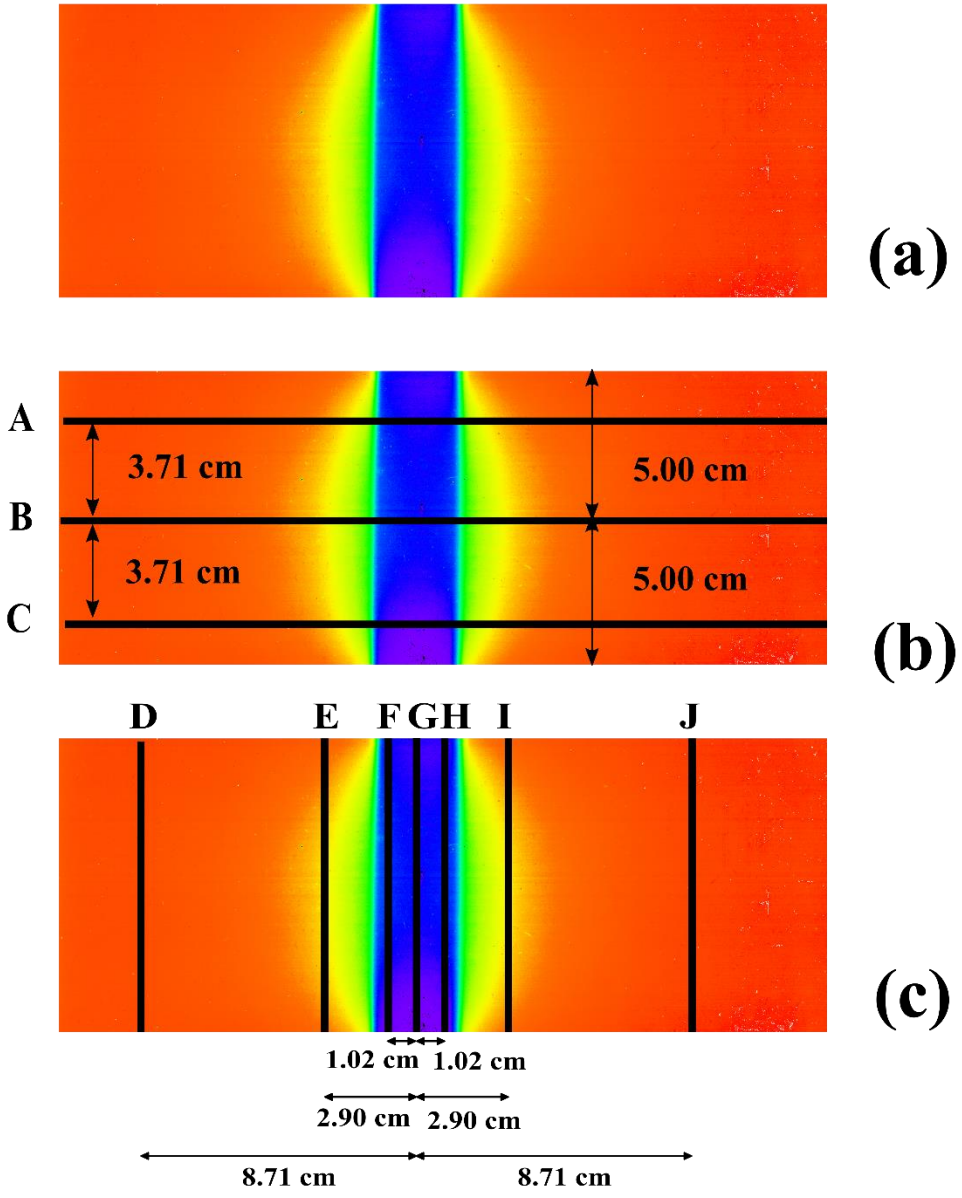

Fig. 3. Pseudo color map of scanned RCF images obtained using phantom 10 cm in diameter (a) and positions of profile curves along the long (b) and short (c) axes.

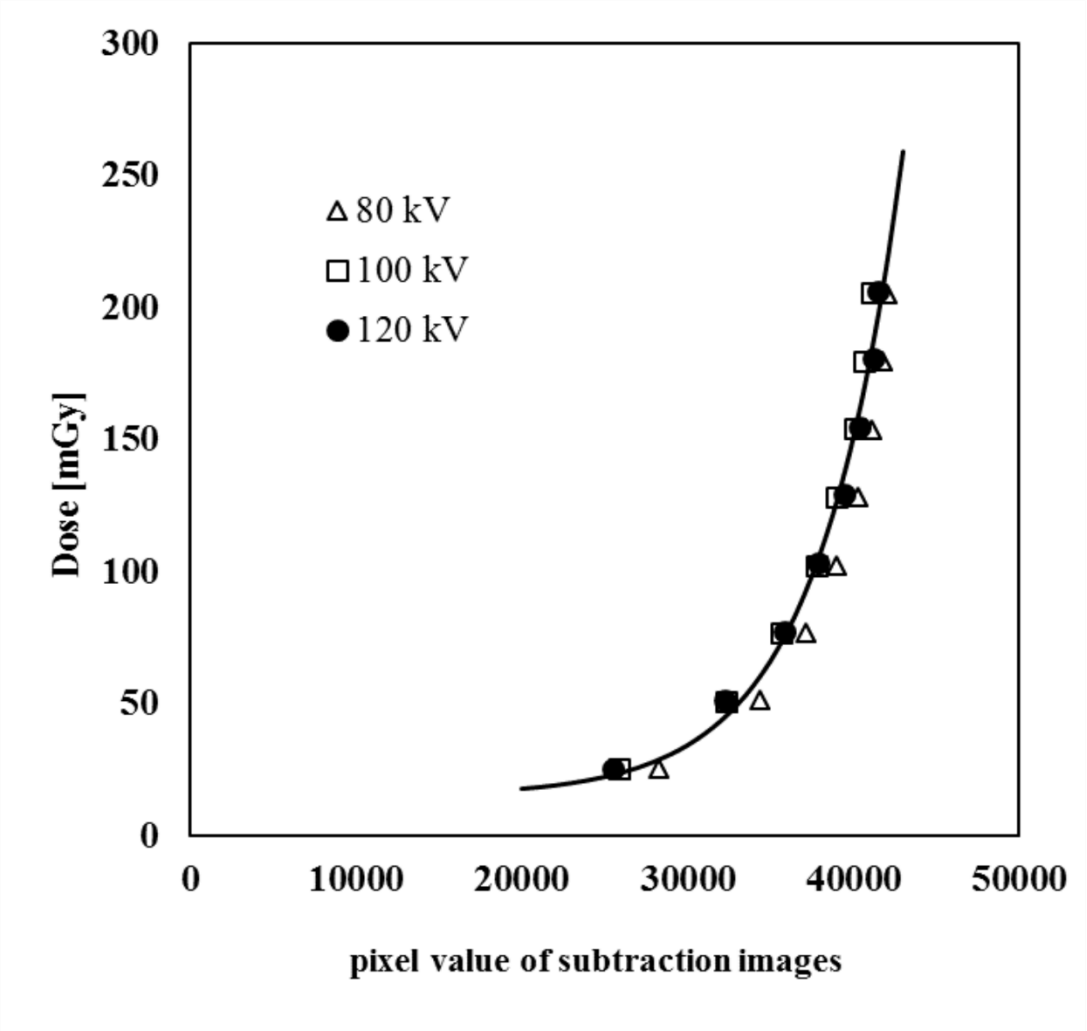

Fig. 4. Dose–pixel value calibration curves for each tube voltage. Pixel values of subtraction images were calculated by subtracting the image after exposure from the image before exposure.

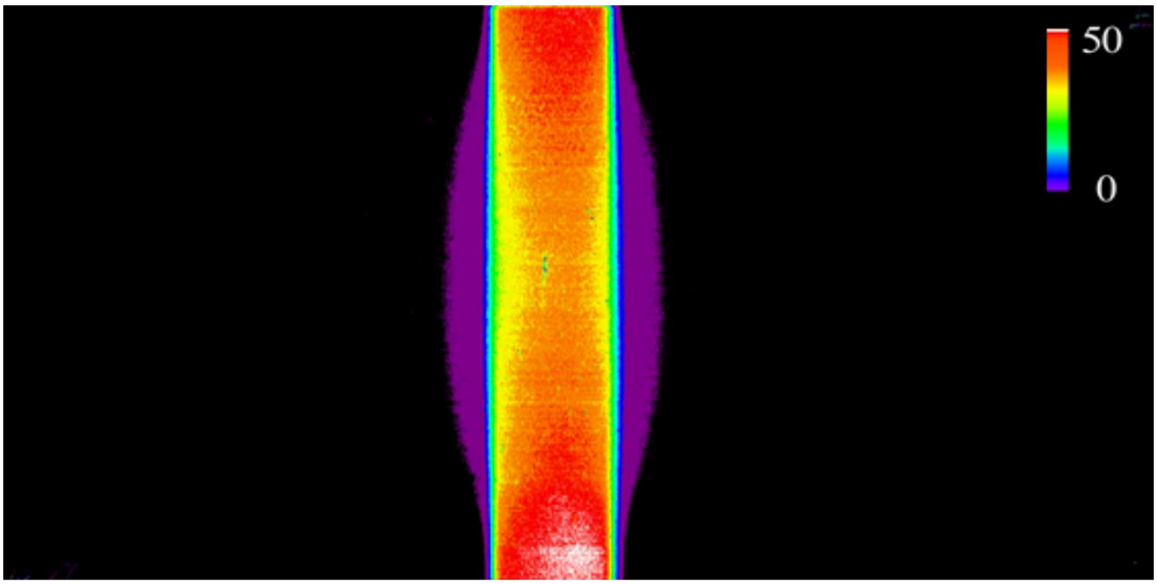

(a)

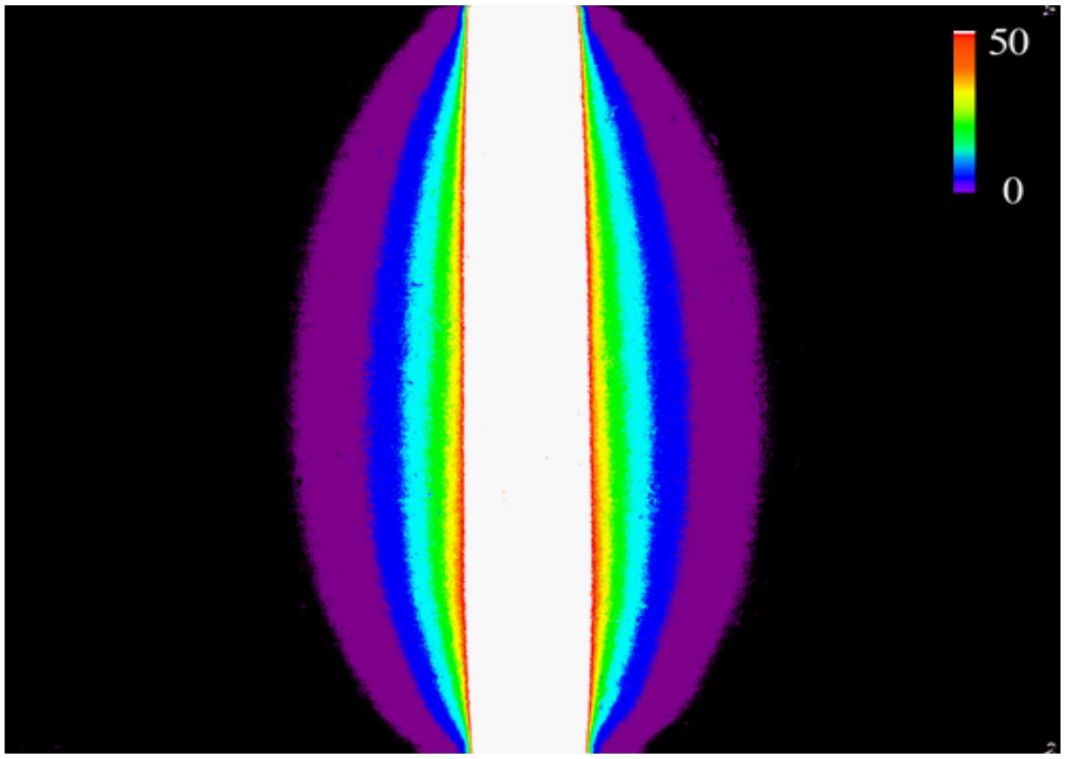

(b)

Fig. 5. Dose distribution map of 10- (a) and 16-cm-diameter phantoms (b)

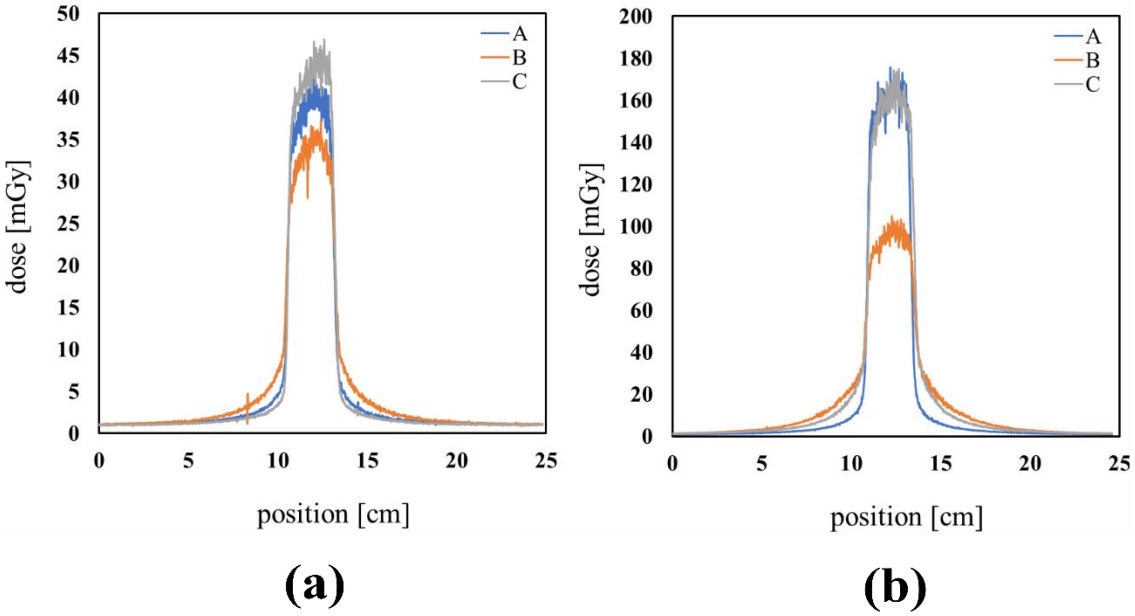

Fig. 6. Dose profile curves along long axis for (a) 10- and (b) 16-cm-diameter phantoms

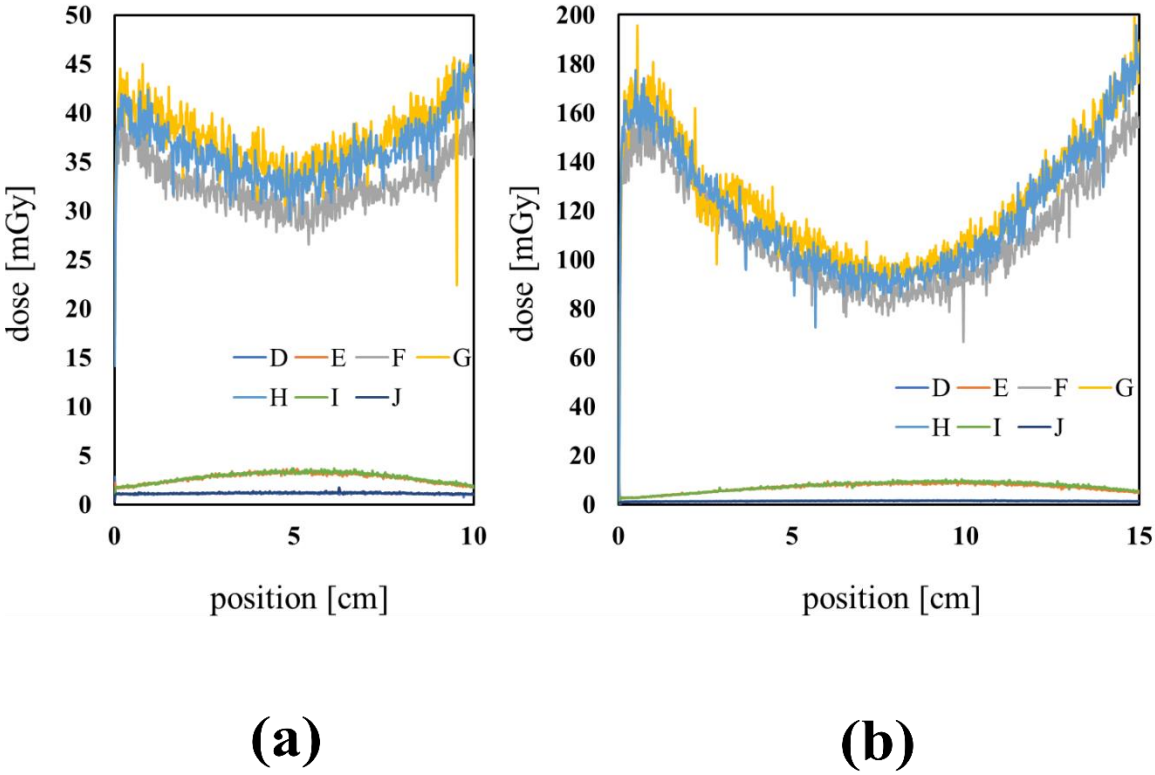

Fig. 7. Dose profile curves along short axis for (a) 10- and (b) 16-cm-diameter phantoms